Journal of
Synchrotron
Radiation

ISSN 1600-5775

Received 14 May 2014
Accepted 25 June 2014

Path degeneracy and EXAFS analysis of disordered materials

Bruce Ravel

National Institute of Standards and Technology, Gaithersburg, MD 20899, USA.
E-mail: bravel@bnl.gov

Analysis of EXAFS data measured on a material with a disordered local configuration environment around the absorbing atom can be challenging owing to the proliferation of photoelectron scattering paths that must be considered in the analysis. In the case where the absorbing atom exists in multiple inequivalent sites, the problem is compounded by having to consider each site separately. A method is proposed for automating the calculation of theory for inequivalent sites, then averaging the contributions from sufficiently similar scattering paths. With this approach, the complexity of implementing a successful fitting model on a highly disordered sample is reduced. As an example, an analysis of Ti *K*-edge data on zirconolite, $CaZrTi_2O_7$, which has three inequivalent Ti sites, is presented.

Keywords: EXAFS; real-space multiple scattering; data analysis.

1. Introduction

In the years since the seminal 1971 paper (Sayers *et al.*, 1971) demonstrating the first practical analysis of the X-ray absorption spectroscopy (XAS) fine structure, XAS has developed into a mature and fully quantitative measurement technique. Since then, the wide proliferation of tools for the analysis of extended X-ray absorption fine structure (EXAFS) has resulted in the application of EXAFS to a broad range of material systems and in a broad range of scientific disciplines. One area where the application of EXAFS analysis remains challenging is to materials which display a high level of structural disorder on the local length scale. For example, the analysis of the EXAFS from a crystalline system is difficult conceptually and procedurally if the absorbing atom sits on two or more unique lattice positions. This paper proposes a useful and readily implemented approximation which simplifies the analysis of the EXAFS on a system with that sort of local disorder.

In the mid-1990s, version 6 of the *FEFF* program (Zabinsky *et al.*, 1995) was introduced. It uses a real-space multiple-scattering formalism to provide reliable theoretical standards for the analysis of the EXAFS. *FEFF* works by computing the effective complex scattering function for any kind of single- or multiple-scattering path and presenting these paths in a way that the EXAFS equation is easily parameterized (Calvin, 2013) in software for quantitative EXAFS analysis.

The *IFEFFIT* package (Newville, 2001), an interactive numerical engine with functionality tailored for use with XAS data, provides the EXAFS functionality for the *ATHENA* (XAS data processing) and *ARTEMIS* (EXAFS data analysis) programs (Ravel & Newville, 2005) and is used throughout this manuscript. There is, however, nothing specific to those software tools in this manuscript. The technique presented here could be implemented in any EXAFS analysis tool which uses *FEFF* as the theoretical backend.

A specific aspect of *FEFF* which makes it so useful for EXAFS analysis is the *path expansion*. Starting with version 6, *FEFF* combined an exhaustive algorithm for enumerating individual scattering paths with an exact separable representation of the photoelectron propagator matrix (Rehr & Albers, 1990). In this way, the measured EXAFS spectrum could be represented as a sum of the contributions from individual scattering geometries in a cluster of atoms. The input to *FEFF* is a list of Cartesian coordinates of atoms centered around an absorbing atom. Its *pathfinder* finds all individual scattering paths with seven or fewer legs. (A two-legged path is a single-scattering path, in which the photoelectron scatters from one, and only one, neighboring atom; a three-legged path is a double-scattering path in which the photoelectron scatters from two, and only two, neighboring atoms; and so on.) The separable representation allows for fast and accurate calculation of the complex scattering function for paths of any order. The contribution from each scattering geometry is then presented for use by the analysis program.

2. The pathfinder

The first chore in *FEFF* related to EXAFS analysis is to compute the muffin-tin potentials using the positions and species of the atoms in the input atomic cluster. *FEFF* then runs its pathfinder to enumerate all possible scattering

geometries within the cluster. Armed with those two results, *FEFF* writes one file per path, each containing the contribution to the EXAFS from a particular scattering geometry.

The algorithm for the pathfinder was presented by Zabinsky *et al.* (1995) and is summarized here. To begin, each single-scattering path, formed by the photoelectron leaving the absorbing atom and scattering from one of the surrounding atoms in the cluster, is noted. Next, double-scattering paths are created from each single-scattering path by extending the single-scattering path to every other atom in the cluster. Each successive higher order of scattering path is constructed by extending the previous order of scattering paths to every atom in the cluster. At each order of scattering, care is taken to reject paths that would include the photoelectron scattering from an atom to the same atom. Scattering paths with four or more legs are allowed to scatter from the absorbing atom as one or more of the interior scattering events. This enumeration is exhaustive; no scattering geometry present in the cluster will be missed.

FEFF next analyzes this ensemble of scattering paths for degeneracy. That is, it flags scattering geometries that will produce identical contributions to the EXAFS. One obvious example of degeneracy is the set of scattering atoms in the first coordination shell of a highly ordered material like copper metal. The 12 nearest neighbors in copper, which crystallizes in the face-centered cubic structure, are all at the same distance and so contribute identically to the EXAFS. Instead of presenting 12 identical scattering paths to the user, *FEFF* presents one path which is flagged as being 12-fold degenerate. Care is taken also to recognize various kinds of geometrical symmetries in multiple-scattering paths, such as time-reversal and mirror.

The paths, flagged for degeneracy, are then sorted by path length. This sorted list is presented for use to the EXAFS analysis program.

3. Fuzzy degeneracy

FEFF is quite strict about its definition of an identical contribution by a scattering path. The level of precision in path length used in *FEFF* is 10^{-5} Å. Two paths that are otherwise identical but which differ in length by only 1 fm are considered non-degenerate by *FEFF*. With rare exception (Pettifer *et al.*, 2005), a 1 fm difference in path length is well below the detection limit of the EXAFS measurement.

The concept of *fuzzy degeneracy* is now introduced. *FEFF*'s pathfinder has been reimplemented to change the behavior of the degeneracy checking at the stage where the heap is collapsed. Instead of requiring strict equality in path length, paths are instead grouped together in bins of a user-supplied width. Single-scattering paths are considered degenerate if their lengths are within that margin. The lengths of the paths in each bin are averaged. The result of collapsing the heap, then, is a list of paths with lengths corresponding to the centers of weight of each bin and with degeneracies equal to the populations of each bin.

The concept of fuzzy degeneracy is extended for multiple-scattering paths by also introducing a margin for scattering angle. Two multiple-scattering paths are considered fuzzily degenerate if they scatter in order from the same atomic species (or in the opposite order, which is known as time-reversal degeneracy), the total path lengths differ by less than the length margin, and each scattering angle differs by less than the angle margin. Each fuzzily degenerate multiple-scattering path has a total path length which is the average of the paths within the bin. Each scattering angle is within the range of scattering angles found in each fuzzily degenerate path. For an arbitrary group of multiple-scattering paths, it may not be possible to average the lengths and the angles and still have the resulting path fit together geometrically. Therefore, the fuzzily degenerate multiple-scattering paths are somewhat less accurately determined than the single-scattering paths. Given the diminished importance of multiple-scattering paths in many problems with large local disorder, this inaccuracy is not a serious shortcoming.

The fuzzily degenerate single-scattering path is characterized by a distance between the absorber and scatterer. The fuzzily degenerate multiple-scattering path is characterized by a set of distances and angles. Using that geometrical information along with the photoelectron scattering factors computed from *FEFF*'s muffin-tin potentials, contributions from each fuzzily degenerate path are generated using *FEFF*'s normal mechanism of representing a path as a file. (This is implemented as a specially crafted version of *FEFF*'s 'paths.dat' file for each fuzzily degenerate path, which is then used to write the output files using *FEFF*'s normal output mechanism.)

4. Fuzzy degeneracy over multiple sites

As an example of both local disorder and the application of fuzzy degeneracy, consider zirconolite, $CaZrTi_2O_7$. This crystallizes (Rossell, 1980) in the monoclinic $C2/c$ space group with three unique lattice positions occupied by Ti, seven by O, and one each by Ca and Zr. To keep the analysis presented here relatively simple, site swapping observed by Rossell (1980) at the level of about 10% between the Zr and Ti_2 sites is neglected. The effect of neglecting site-swapping will be addressed in §5.

There are eight Ti_1 atoms in the unit cell, and four each of Ti_2 and Ti_3. Thus a half of all Ti atoms are in site 1 and one-quarter each in sites 2 and 3. Each Ti site is surrounded by six oxygen atoms at the distances shown in Table 1. Degeneracies are computed fuzzily over the sites and degenerate paths are weighted by the fractional population of each site in the unit cell. The bin size for the analysis presented below was chosen as 0.1 Å. This results in the four paths with average distances and non-integer degeneracies given in the left-most column of Table 2. The $\chi(k)$ spectra computed from each strictly degenerate path and each fuzzily degenerate path are shown in the top panel of Fig. 1.

Table 1
Strict degeneracies and lengths (Å) of the near-neighbor oxygen single-scattering paths for each of the three Ti sites in $CaZrTi_2O_7$.

Data are from the structure reported by Rossell (1980).

Ti_1	Ti_2	Ti_3
1@1.843	2@1.786	2@1.875
1@1.880	2@2.050	2@1.877
1@1.927	2@2.498	2@1.975
1@1.987		
1@2.007		
1@2.023		

Table 2
Fuzzy degeneracies and average lengths (Å) of the paths for each scatterer type, up to 4.0 Å.

There is a path with 0.5 Ti atoms just beyond the cut-off distance of 4.0 Å. These paths are parameterized as explained in the text. The sums of the contributions from each scatterer are shown in Fig. 3.

O	Ca	Zr	Ti	O
2.5@1.852	0.5@3.114	1.0@3.275	0.5@3.113	0.5@3.193
2.5@1.984	2.0@3.466	1.0@3.636	1.0@3.364	1.0@3.639
0.5@2.050	0.5@3.542	1.0@3.756	3.0@3.615	2.5@3.738
0.5@2.498			1.0@3.901	2.5@3.850
				1.5@3.944

The middle panel of Fig. 1 shows the sums of the $\chi(k)$ spectra for the strictly and fuzzily degenerate paths. The binning of nearly degenerate paths serves to slightly reduce the static disorder of the paths. This can be seen by the small enhancement of $\chi(k)$ for the sum of the fuzzily degenerate paths in the middle panel. The bottom panel shows the Fourier transforms of the sums of the strictly and fuzzily degenerate paths, again with a small enhancement of the fuzzily degenerate signal due to the reduction in static disorder. Those two panels together show that fuzzy degeneracy over sites is an accurate approximation of the strictly degenerate calculation. This small change in static disorder will result in a small change in the value of σ^2 determined from the fit.

Scattering paths from the near-neighbor Ca, Zr, Ti and more distant O atoms are also widely distributed when counted with strict degeneracy, resulting in 51 single-scattering paths with path length below 4.0 Å from the three Ti positions. By considering degeneracy fuzzily with a margin of 0.1 Å and over all three sites, these 51 paths are collapsed to just 19. While it is still substantial work to manage even 19 paths in data analysis software, the scale of problem is much diminished with scant impact on the accuracy of the calculation, as shown in the lower panels of Fig. 1.

5. EXAFS analysis using fuzzy degeneracy

Data were measured on the Ti *K*-edge of $CaZrTi_2O_7$ at beamline X23A2 of the National Synchrotron Light Source. This is an unfocused bend-magnet beamline using an Si(311) monochromator of a fixed-exit Golovchenko–Cowan (Golovchenko *et al.*, 1981) design. Harmonic rejection is made

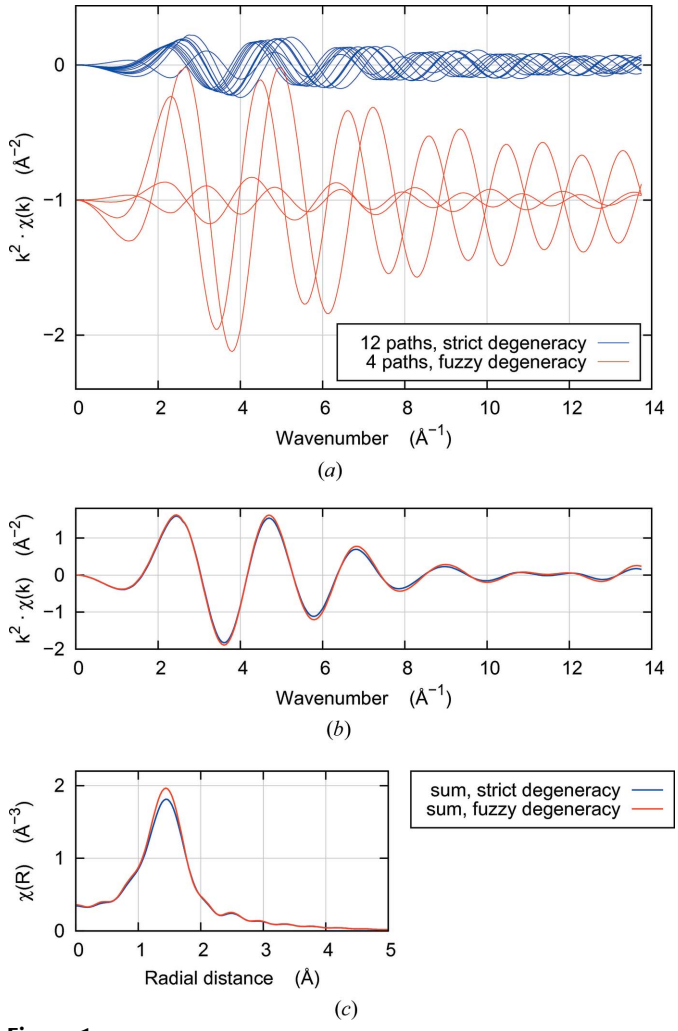

Figure 1
(*a*) Three Ti sites contribute a total of 12 oxygen single-scattering paths, shown in blue, with lengths and degeneracies shown in Table 1. With a binning width of 0.1 Å, these are reduced to four fuzzily degenerate paths, shown in red and offset downward for clarity, with lengths and degeneracies shown in Table 2. As plotted here, each path is evaluated with S_0^2 set to 1 and each of E_0, ΔR and σ^2 set to 0. (*b*) Sum of the 12 strictly degenerate paths in blue, compared with the sum of the four fuzzily degenerate paths. Note that interference between paths of different lengths results in substantial attenuation of the signal above 7 Å^{-1}. (*c*) Fourier transforms of the summed $\chi(k)$ spectra.

by a single-bounce flat Rh-coated mirror. The incident and transmitted X-ray intensities were measured using N_2-filled ionization chambers. A fine powder was mixed with polyethylene glycol and pressed into a thin rigid pellet. Four EXAFS scans were obtained in transmission mode and averaged for analysis. Raw data were processed using the *ATHENA* program and are shown in Fig. 2. EXAFS analysis was performed using *FEFF6* and the *ARTEMIS* program.

Although the scale of this analysis problem has been reduced substantially using fuzzy degeneracy, this remains a problem severely constrained by limited information. The *k*-range over which the data is Fourier transformed is 3 to 10.5 Å^{-1} and the fit is evaluated over a range of 1 to 4 Å. By the Nyquist criterion (Brillouin, 1962), this gives at most 15.3 independent data points.

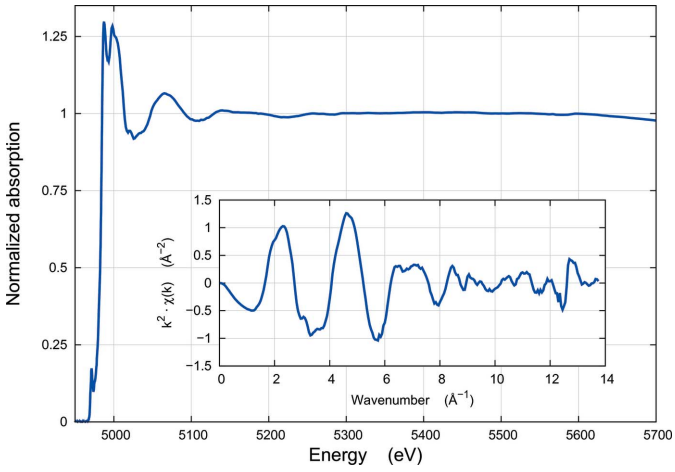

Figure 2
Normalized $\mu(E)$ data measured on the $CaZrTi_2O_7$ sample. (Inset) Extracted k^2-weighted $\chi(k)$ data.

As with any EXAFS analysis, we start with the EXAFS equation for the contribution from a single-scattering path,

$$\chi_\Gamma(k) = \frac{NS_0^2 F_\Gamma(k)}{2kR_\Gamma} \exp(-2k^2\sigma_\Gamma^2) \exp[-2R_\Gamma/\lambda(k)] \times \sin\left[2kR_\Gamma + \delta_\Gamma(k)\right]. \quad (1)$$

Here, Γ is an index counting over all scattering paths considered in the fit. $F_\Gamma(k)$ and $\delta_\Gamma(k)$ are the amplitude and phase of the photoelectron scattering function and are computed by *FEFF*, as is $\lambda(k)$, the photoelectron mean free path. The remaining terms [N is the path degeneracy, S_0^2 is the passive electron reduction factor (Li *et al.*, 1995), R is the scattering path length and σ^2 is the mean-square variation in scattering path length] are all parameterized using the variables of the fit. Additionally, an energy shift parameter, E_0, is used to modify the zero of photoelectron wavenumber k when fitting theory to data. In this case, $\chi_\Gamma(k)$ and all the terms in the EXAFS equation are evaluated using the binned, fuzzily degenerate paths. Finally, all paths used in the analysis are summed,

$$\chi_{\rm theory}(k) = \sum_\Gamma \chi_\Gamma(k), \quad (2)$$

and compared with the measured $\chi(k)$. See Calvin (2013) for a thorough explanation of EXAFS analysis.

A simple model is used to parameterize these paths for the fit. The values for degeneracy from Table 2 were fixed. Values for S_0^2 and E_0 are varied and are constrained to be the same for each path. Five ΔR parameters are defined, one for the O atoms in the first shell, one for the remaining O atoms and one for each metal scatterer. Except for the near-neighbor O scatterers, each fuzzily degenerate path is constrained to have the same ΔR parameter as the other paths from the same scattering species. Thus, the ΔR parameter for the metal and distant oxygen atoms is interpreted as a shift of the center of weight of the distribution. For the near-neighbor O scatterers, $\Delta R_{\rm O}$ was applied to the shorter two paths and $-\Delta R_{\rm O}$ was applied to the longer two paths. Thus $\Delta R_{\rm O}$ serves to narrow the distribution without shifting its center of weight. The fit was statistically significantly improved by applying $\Delta R_{\rm O}$ in this manner rather than as a shift to the center of weight of the distribution.

Table 3
Fitted parameter values for the fit shown in Fig. 3.

E_0 has units of eV, ΔR parameters have units of Å, and σ^2 parameters have units of 10^{-5} Å^2. 1σ uncertainties, determined from the fit, are shown in parentheses.

$S_0^2 = 0.824\ (147)$	$E_0 = -3.93\ (169)$
$\sigma^2_{\rm O} = 246\ (299)$	$\Delta R_{\rm O} = -0.001\ (14)$
$\sigma^2_{\rm Ti} = 525\ (434)$	$\Delta R_{\rm Ti} = -0.014\ (31)$
$\sigma^2_{\rm Zr} = 414\ (600)$	$\Delta R_{\rm Zr} = -0.042\ (43)$
$\sigma^2_{\rm Ca} \equiv \sigma^2_{\rm Ti}$	$\Delta R_{\rm Ca} = -0.223\ (36)$
$\sigma^2_{\rm O_2} = 453\ (958)$	$\Delta R_{\rm O_2} = 0.095\ (54)$

Four σ^2 parameters are defined, one for the O atoms in the first shell, one for the remaining O atoms, and one each for the Ti and Zr scatterers. The σ^2 value for the Ca scatterers is constrained to be the same as for the Ti scatterers since these two atoms are of similar mass. This results in a total of 11 parameters to be determined from the fit (see Table 3).

At 11 parameters, this model places considerable strain on the information content of the data. Because of this information limit, it is impractical to expect detailed results about the distribution of the many scatterers about the Ti absorbers. The parameters used in this fit should be interpreted as changes to the centroids and widths of the five distributions of scatterers. Because these distributions are computed over the three Ti sites, this parameterization is hard to interpret in a crystallographic context except insofar as the crystallographic structure might be consistent with the measured EXAFS data.

The value of S_0^2 is reasonable (Li *et al.*, 1995). The E_0 value is small, indicating the zero of k was well chosen during removal of the background from the $\mu(E)$ data.

The ΔR parameters, except for the Ca scatterers, are mostly consistent with zero and rather small, indicating that the distributions in the crystal data are quite consistent with these EXAFS data. The centroid of the Ca scatterers, however, is shifted to a substantially lower distance. Given this large shift, it would be prudent to recompute the contribution of the Ca scatterers. This, however, cannot be automated in the current version of the software used for this analysis. The inaccuracy of the backscattering function with such a large shift therefore contributes systematic error to the analysis.

The σ^2 parameters are a bit more ambiguous. While all are of a size expected for thermal mean-square disorder, all but one have uncertainties larger than their values. This ambiguity in σ^2 is understood by examination of the correlations between parameters and in light of the approximations that enter the fitting model. Substantial correlations in excess of 40% are found between several of the ΔR and σ^2 parameters. As seen in Fig. 3, the spectral weights from the different scattering atoms overlap, thus the fit throughout the range from 2.5 to 4 Å depends upon the superposition of these signals. Complicating these interactions are two significant approximations made in this fitting model. First, the effect of

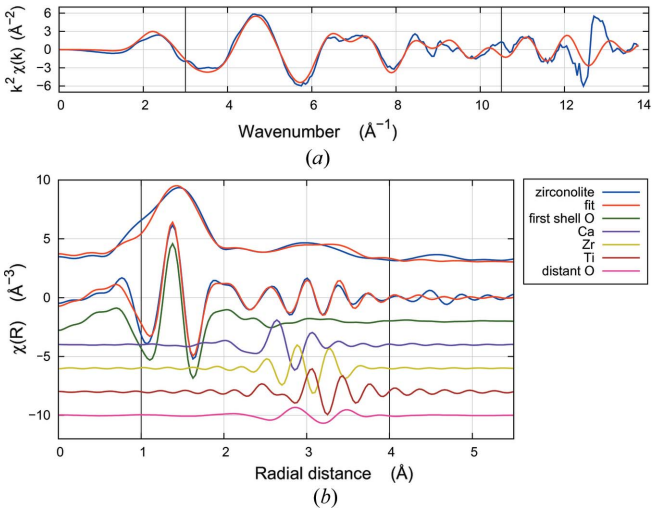

Figure 3
Fit to the $CaZrTi_2O_7$ sample. The result of the fit is shown as $\chi(k)$ in (*a*) and as the magnitude and real part of $\tilde{\chi}(R)$ in (*b*). Also shown are the real parts of $\tilde{\chi}(R)$ for the sums of the fuzzily degenerate paths from each scattering species, which are enumerated in Table 2. Fourier transform and fitting ranges are shown by the vertical bars in each panel.

site swapping has been neglected. In the paper by Rossell (1980), the predominant site swapping is between Ti and Zr, two atoms of very different mass. As a result, the correlations between the ΔR and σ^2 parameters related to Ti and Zr are all high. Additionally, the effect of various triangle-shaped multiple-scattering paths has been neglected in this analysis. Such paths, though small, contribute in the range 2.5 to 4 Å, exactly where the highly correlated parameters impact upon the fit. So their absence certainly contributes somewhat to the ambiguity in the determination of the σ^2 parameters.

Lifting the constraint on σ^2 for the Ca scatterer yields no statistically significant improvement to the fit. While this parameter cannot be independently and defensibly determined, this constraint certainly further contributes to the ambiguity of the results on the σ^2 values.

As a check on the reasonableness of the ΔR value for the near-neighbor O atoms, a bond-valence sum (Brown & Altermatt, 1985) is computed using the fitted path lengths of the four near-neighbor oxygen paths and their non-integer degeneracies (see Table 2). The sum evaluates to 4.199 ± 0.153, quite consistent with the Ti^{4+} valence state (Rossell, 1992) in $CaZrTi_2O_7$.

With severe constraints on the information content of the data and with ambiguities in many of the σ^2 parameters, this is far from an ideal example of EXAFS analysis. The data are found to be substantively consistent with the known crystal structure, but detailed information about the partial pair distributions of atoms around the Ti absorber cannot be extracted from analysis of these data. Still, this is a useful result. The material which provides the example of this methodology also provides an example of its utility. Zirconolite is used as a storage medium for actinide waste, including uranium and other tetravalent actinides (Kessoft *et al.*, 1983; Vance *et al.*, 2002). Over time, the host material is amorphized by damage from energetic alpha particles emitted by radioactive decay of the actinide. This amorphization is readily visible in the XAS spectrum (Reid *et al.*, 2010). The methodology presented here provides a practical way of quantifying the effect of alpha-recoil amorphization of differently aged samples by measuring changes over the ensemble in the fitted parameter values.

6. Discussion

The motivation for the methodology presented in this paper is the management of a class of difficult EXAFS analysis problems. $CaZrTi_2O_7$ has the absorbing Ti atoms in multiple, inequivalent crystallographic sites with considerable disorder in the local configuration environment. This results in a proliferation of scattering paths that must be considered in the EXAFS analysis. The solution presented here is to define path degeneracy fuzzily and over all sites. Paths are calculated from all sites and those of similar length are presented together to the user of the data analysis software. The degeneracy of these paths may be non-integer and reflects the population of each crystallographic site in the unit cell. By condensing the proliferation of paths in this way, the complexity of the EXAFS analysis problem is significantly reduced.

An additional complicating factor to analysis of data from a material like $CaZrTi_2O_7$ is that the information content of the data typically is severely limited compared with the amount of information one might hope to extract from the analysis. In this case, the data contained barely more than 15 independent data points. The Ti EXAFS data in $CaZrTi_2O_7$ must, however, consider the scattering from Ca atoms, Zr atoms, other Ti atoms, and O atoms in two distinct distance ranges. Fuzzy degeneracy is, therefore, a tool to simplify the analysis problem in the face of these challenges.

There is a pitfall to the use of fuzzy degeneracy. Given that EXAFS data are measured over a limited range in k-space, there is a natural limit to the spatial resolution, the ability to resolve differences in length of two scattering paths δR, given as $\delta R = \pi/(2\Delta k)$, where Δk is the extent of the k-range used in the Fourier transform. The width of the bin used for the fuzzy degeneracy places a limit on the spatial resolution of the theory. The bin width should not be larger than the spatial resolution determined by the k-range of the data.

There are other ways of approximating contributions from highly disordered partial pair distribution functions in an EXAFS analysis problem. The *GNXAS* package (Filipponi *et al.*, 1995) allows the user to integrate the contribution of a scattering atom over a user-defined analytic distribution function. While this is likely to be more accurate than the procedure presented here, it requires prior knowledge of the analytic form of the function, which is certainly not the case in this example. A partial pair distribution function can be approximated using a cumulant expansion (Bunker, 1983). This, however, tends to introduce additional fitting parameters when the measured disorder has a large static component in addition to the purely thermal (Frenkel & Rehr, 1993) component. The purpose of this manuscript is to offer a

mechanism to reduce the total number of fitting parameters required.

The reason higher cumulants can be neglected in the fit when using fuzzy degeneracy is that the fuzzily degenerate paths retain considerable static disorder so long as the margin for the determination of the fuzzy degeneracy is not too large. In the case of $CaZrTi_2O_7$, a margin of 0.1 Å retains most of the static disorder of the set of strictly degenerate paths, as shown in Fig. 1. In this case, given the extent of the structural disorder, these distributions would be poorly approximated by a small number of cumulants.

While the example shown here involves a crystal with the absorbing atom in multiple crystallographic sites, this procedure is readily adapted to noncrystalline materials for which a structure is known. For example, a metalloprotein with distinct active sites could be treated in the manner presented here by first finding all paths about each distinct site, then forming fuzzily degenerate paths over the sites.

A few words about the implementation of the algorithms presented here are offered in closing. While reference has been made specifically to version 6 of the *FEFF* program, the algorithm for enumerating EXAFS scattering paths is unchanged in later versions. This procedure for making fuzzily degenerate paths is applicable to any version of *FEFF*. The automated enumeration of fuzzily degenerate paths, including enumeration over multiple sites in a crystal, is available in recent versions of the *ARTEMIS* program. The width of the degeneracy margin is a user-configurable parameter in *ARTEMIS*.

The author thanks D. Reid, M. Stennett and N. Hyatt of the University of Sheffield for graciously donating their zirconolite data. Use of the National Synchrotron Light Source, Brookhaven National Laboratory, was supported by the US Department of Energy, Office of Science, Office of Basic Energy Sciences, under contract No. DE-AC02-98CH10886.

References

Brillouin, L. (1962). *Science and Information Theory*. New York: Academic Press.
Brown, I. D. & Altermatt, D. (1985). *Acta Cryst.* B**41**, 244–247.
Bunker, G. (1983). *Nucl. Instrum. Methods Phys. Res.* **207**, 437–444.
Calvin, S. (2013). *XAFS for Everyone*. Boca Raton: CRC Press.
Filipponi, A., Di-Cicco, A. & Natoli, C. R. (1995). *Phys. Rev. B*, **52**, 15122–15149.
Frenkel, A. & Rehr, J. (1993). *Phys. Rev. B*, **48**, 585–588.
Golovchenko, J., Levesque, R. & Cowan, P. (1981). *Rev. Sci. Instrum.* **52**, 509–516.
Kessoft, S., Sinclair, W. & Ringwood, A. (1983). *Nucl. Chem. Waste Manag.* **4**, 259–265.
Li, G., Bridges, F. & Booth, C. (1995). *Phys. Rev. B*, **52**, 6332–6348.
Newville, M. (2001). *J. Synchrotron Rad.* **8**, 322–324.
Pettifer, R. F., Mathon, O., Pascarelli, S., Cooke, M. D. & Gibbs, M. R. (2005). *Nature (London)*, **435**, 78–81.
Ravel, B. & Newville, M. (2005). *J. Synchrotron Rad.* **12**, 537–541.
Rehr, J. J. & Albers, R. C. (1990). *Phys. Rev. B*, **41**, 8139–8149.
Reid, D., Stennett, M., Ravel, B., Woicik, J., Peng, N., Maddrell, E. & Hyatt, N. (2010). *Nucl. Instrum. Methods Phys. Res. B*, **268**, 1847–1852.
Rossell, H. (1980). *Nature (London)*, **283**, 282–283.
Rossell, H. (1992). *J. Solid State Chem.* **99**, 38–51.
Sayers, D. E., Stern, E. A. & Lytle, F. W. (1971). *Phys. Rev. Lett.* **27**, 1204–1207.
Vance, E. R., Lumpkin, G. R., Carter, M. L., Cassidy, D. J., Ball, C. J., Day, R. A. & Begg, B. D. (2002). *J. Am. Ceram. Soc.* **85**, 1853–1859.
Zabinsky, S. I., Rehr, J. J., Ankudinov, A., Albers, R. C. & Eller, M. J. (1995). *Phys. Rev. B*, **52**, 2995–3009.